ARTICLE
PUBLISHED ONLINE: 25 MAY 2015 | DOI: 10.1038/NCHEMBIO.1817

Prolonged and tunable residence time using reversible covalent kinase inhibitors

J Michael Bradshaw[1]*, Jesse M McFarland[2], Ville O Paavilainen[2], Angelina Bisconte[1], Danny Tam[1], Vernon T Phan[1], Sergei Romanov[3], David Finkle[1], Jin Shu[1], Vaishali Patel[1], Tony Ton[1], Xiaoyan Li[1], David G Loughhead[1], Philip A Nunn[1], Dane E Karr[1], Mary E Gerritsen[1], Jens Oliver Funk[1], Timothy D Owens[1], Erik Verner[1], Ken A Brameld[1], Ronald J Hill[1], David M Goldstein[1] & Jack Taunton[2]*

Drugs with prolonged on-target residence times often show superior efficacy, yet general strategies for optimizing drug-target residence time are lacking. Here we made progress toward this elusive goal by targeting a noncatalytic cysteine in Bruton's tyrosine kinase (BTK) with reversible covalent inhibitors. Using an inverted orientation of the cysteine-reactive cyanoacrylamide electrophile, we identified potent and selective BTK inhibitors that demonstrated biochemical residence times spanning from minutes to 7 d. An inverted cyanoacrylamide with prolonged residence time *in vivo* remained bound to BTK for more than 18 h after clearance from the circulation. The inverted cyanoacrylamide strategy was further used to discover fibroblast growth factor receptor (FGFR) kinase inhibitors with residence times of several days, demonstrating the generalizability of the approach. Targeting of noncatalytic cysteines with inverted cyanoacrylamides may serve as a broadly applicable platform that facilitates 'residence time by design', the ability to modulate and improve the duration of target engagement *in vivo*.

Drug discovery programs historically have sought to optimize molecules by maximizing the thermodynamic affinity (i.e., K_d or half-maximal inhibitory concentration (IC_{50})) of the drug-target interaction. Less attention has been given to the drug residence time (τ)[1], which is defined as the inverse of the off rate (k_{off}) such that $\tau = 1/k_{off}$. Recently, it has become clear that drug-target residence time, rather than affinity, often drives pharmacodynamic activity and disease efficacy *in vivo*[2–4]. Hence, residence time should be a key area of focus during the drug discovery process[5–7]. A current lack of systematic approaches for the design of molecules with slow off rates has hindered efforts to discover drugs with prolonged residence times.

Inhibitors that form a reversible covalent bond with a noncatalytic cysteine of the target may prove widely applicable for obtaining prolonged residence times. An approach to the discovery of such inhibitors was recently reported[8,9]. In that work, a cyanoacrylamide electrophile attached to a kinase-recognition scaffold was designed to form a covalent but fully reversible bond with Cys436 in the C-terminal kinase domain of RSK2. These cyanoacrylamide inhibitors provided sustained engagement of RSK2, with biochemical residence times of up to 6 h (ref. 9). Despite these promising results, it remained unclear how residence time could be systematically modulated. Moreover, characterization of cyanoacrylamide-based kinase inhibitors has to date focused on biochemical and cellular systems, and whether such inhibitors demonstrate prolonged residence times *in vivo* after oral administration has not been established.

Reversible covalent drugs have at least two theoretical advantages over their irreversible counterparts. First, relative to reversible covalent drugs, drugs that rely on intrinsically irreversible chemistry (for example, acrylamides) are more likely to form permanent covalent adducts[10–12] with off-target proteins, including both closely related targets (for example, off-target kinases with a homologous cysteine) and unrelated targets with hyper-reactive cysteines[13]. Second, and equally important, reversible cysteine engagement may enable fine tuning of the inhibitor residence time, a feature that would facilitate the use of such inhibitors not only in therapeutic applications requiring sustained target engagement, but also in applications where more rapid target disengagement is preferred[2]. As many drug targets, including kinases[14–16], have an accessible cysteine in their binding site, there is broad opportunity to discover reversible covalent inhibitors for use across many therapeutic areas.

BTK contains a noncatalytic cysteine (Cys481) that is the target of several inhibitors[17–23]. Among these compounds, ibrutinib[17] is particularly noteworthy and was recently approved for treatment of the B cell malignancies chronic lymphocytic leukemia[24] and mantle cell lymphoma[25]. Selective BTK inhibitors have also shown activity in collagen-induced arthritis and other rodent models of inflammation[17,19,26,27], providing a rationale for BTK inhibition in autoimmune diseases. Given that irreversible acrylamide-based kinase inhibitors, including ibrutinib, have been shown to form permanent covalent adducts with kinase and non-kinase off-target proteins[28], it is not clear whether such compounds have the requisite selectivity profile for use in autoimmune diseases, which typically require chronic dosing and a high safety margin.

Here we explored the possibility of engaging BTK Cys481 with reversible covalent inhibitors. Inverting the orientation of the cyanoacrylamide relative to the kinase active site and perturbing the steric and electronic environment of the electrophilic carbon led to the discovery of inhibitors with remarkably slow off rates. These inhibitors had biochemical residence times of up to 7 d and illustrate the feasibility of fine-tuning inhibitor residence times on BTK across a wide dynamic range. An inhibitor that was orally bioavailable also demonstrated sustained BTK occupancy *in vivo*. The prolonged residence times and excellent kinase selectivity profiles of these inhibitors suggest potential applications in chronic

[1]Principia Biopharma, South San Francisco, California, USA. [2]Department of Cellular and Molecular Pharmacology and Howard Hughes Medical Institute, University of California, San Francisco, California, USA. [3]Nanosyn Inc., Santa Clara, California, USA. *e-mail: michael.bradshaw@principiabio.com or jack.taunton@ucsf.edu

inflammatory diseases. The inverted-cyanoacrylamide approach was further applied to an entirely different kinase and cysteine position (FGFR1 Cys486), and this also resulted in inhibitors with prolonged and tunable residence times, illustrating broad applicability of the strategy for numerous drug targets.

RESULTS

Design of reversible covalent BTK inhibitors

Structure-based design was used to identify lead molecules starting with scaffolds for which BTK crystallographic binding modes had been reported (**Supplementary Results**, **Supplementary Fig. 1**)[29,30]. A key challenge was identifying an accessible vector to Cys481 that could accommodate a reversible cyanoacrylamide-based electrophile. A previous design strategy[8,9]—linking the electrophilic β-carbon directly to a kinase-recognition scaffold—seemed suboptimal, as Cys481 is located outside the ATP binding site. To solve this problem, we inverted the cyanoacrylamide relative to the scaffold, orienting the electrophilic β-carbon toward the protein surface, distal to the active site. This new orientation provided unexpected opportunities for modulating residence time. First, it allowed us to explore multiple vectors to a common pyrazolopyrimidine scaffold by coupling geometrically diverse amine-containing linkers to the cyanoacrylamide carboxyl group. Second, it made it possible to manipulate the steric and electronic environment of the electrophilic β-carbon through the use of branched-alkyl capping groups (**Fig. 1a**).

To test whether alkyl capping groups with increased branching and steric size confer prolonged residence time, we prepared cyanoacrylamides **1**–**3** bearing a piperidine linker and a pyrazolopyrimidine scaffold (**Fig. 1a**). Cyanoacrylamides with branched-alkyl capping groups are unique; the vast majority of cyanoacrylamides contain aromatic or heteroaromatic β-substituents (including previously reported reversible covalent kinase inhibitors[8,9]). Despite having similar potency in a cellular BTK-occupancy assay under continuous exposure (**Supplementary Fig. 2**), compounds **1**–**3** showed distinct BTK residence times. This was assessed after extensive washing of compound-treated Ramos B cells that were then labeled with a pyrazolopyrimidine fluorescent probe (referred to here as PP-BODIPY) previously shown to penetrate cells and covalently bind BTK with high selectivity[17]. The *tert*-butyl–capped variant **3** had the longest residence time, showing 55% BTK occupancy 20 h after washout (**Fig. 1b**). The other inhibitors showed significantly reduced (**2**) or negligible (**1**) BTK occupancy after 20 h, demonstrating that the durability of these cyanoacrylamides can be modulated through alterations to the capping group.

To obtain molecular insight into the prolonged occupancy of **3**, we solved its co-crystal structure bound to the BTK kinase domain at 2.2-Å resolution. The electron density enabled unambiguous ligand placement (**Supplementary Fig. 3**), revealing strong density for the covalent bond and the formation of two sp^3-hybridized carbons resulting from Cys481 addition to Cβ and protonation of Cα (**Fig. 1c**). Examination of the torsion angles and interactions surrounding this region revealed structural features that probably contribute to the prolonged residence time. To minimize 1,3-torsional strain and steric clashes with the protein, both the *tert*-butyl capping group and the piperidine amide are oriented so as to shield the critical proton attached to Cα, which must be removed before (or during) elimination of the Cys481 thiol (**Fig. 1c**). Moreover, this conformation prevents overlap between the Cα-H bond and the carbonyl π-system and therefore should reduce the kinetic and thermodynamic acidity[31] of the Cα-H bond and hence the rate of Cys481 elimination. Interactions between the *tert*-butyl capping group and a hydrophobic patch near Cys481, as well as a hydrogen bond between the amide carbonyl of **3** and the backbone NH of Cys481, may further stabilize the covalent complex. Consistent with the concept that these and other noncovalent interactions

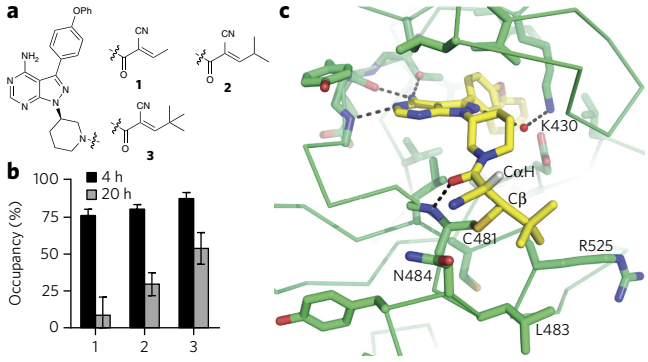

Figure 1 | Reversible covalent BTK inhibitors based on inverted cyanoacrylamides. (**a**) Cyanoacrylamides, attached via a piperidine linker to a pyrazolopyrimidine scaffold, were capped with alkyl groups of increasing steric demand (**1**–**3**). (**b**) Inhibitors **1**–**3** showed distinct levels of BTK occupancy in cells after inhibitor washout. Ramos B cells were treated with DMSO or compound (1 μM) for 1 h, washed three times with PBS and incubated in compound-free medium at 37 °C. After 4 or 20 h, cells were treated with 1 μM PP-BODIPY (an irreversible probe that labels BTK Cys481) for 1 h and then lysed and analyzed by in-gel fluorescence. Occupancy was calculated as 100% minus the normalized in-gel fluorescence intensity divided by the DMSO control value (mean ± s.d., n = 3). (**c**) Co-crystal structure of **3** bound to BTK at 2.2-Å resolution. The covalent bond between Cys481 and Cβ, newly formed CαH and select hydrogen bonds are indicated. Two of the capping-group methyls formed hydrophobic contacts with Leu483 and Arg525, whereas the third was solvent exposed.

with the folded kinase domain have an essential role in kinetic trapping of the complex, guanidine-mediated unfolding resulted in rapid regeneration of **3** in 88% ± 10% yield (**Supplementary Fig. 4**). Finally, the structure revealed that one of the *tert*-butyl methyl groups is solvent exposed, providing a site for the attachment of polar substituents that could potentially improve aqueous solubility.

BTK residence time modulated over a wide dynamic range

Although **3** demonstrated sustained BTK occupancy in both cellular and biochemical assays (**Supplementary Fig. 5a**) and was highly selective against other kinases with a structurally homologous cysteine (>1,000-fold selectivity vs. EGFR and JAK3 and 60-fold selectivity vs. ITK; **Supplementary Fig. 5b**), its low solubility and poor oral bioavailability prompted exploration of structural modifications throughout the molecule, with a primary focus on the linker and capping group. These efforts, which included substitutions on the scaffold (for example, monofluorination) and installation of a more flexible linker, led to the identification of **4** as a starting point for modulating BTK residence time (**Fig. 2a**). To bracket both extremes of the residence-time spectrum, we also synthesized an acrylamide variant of **4** expected to bind irreversibly (**5**, PP-ir) and a nonelectrophilic variant expected to have a rapid off rate (**6**, PP-ne) (**Fig. 2a**).

To facilitate the detection of subtle differences in inhibitor residence times, we developed a kinetic-competition assay using recombinant, full-length BTK (**Supplementary Fig. 6**). The assay measures the length of time that an inhibitor prevents binding of a high-affinity fluorescent tracer added in large excess[32–34]. Inhibitor potency was also determined using a conventional enzymatic-activity assay. Inhibitor **4** demonstrated high potency (IC_{50} = 1.4 ± 0.2 nM; **Supplementary Fig. 7**) and gradually dissociated from BTK over many hours at room temperature (τ = 22 ± 3 h) (**Fig. 2b**), suggesting that it forms a covalent but reversible bond with Cys481. In contrast, the acrylamide-containing inhibitor PP-ir showed no

evident dissociation, suggesting irreversible cysteine engagement. The compound lacking an electrophile, PP-ne, was less potent (IC_{50} = 170 ± 50 nM) and dissociated within 5 min (**Fig. 2c**). Dasatinib, a potent noncovalent BTK inhibitor[35] (IC_{50} = 0.5 ± 0.1 nM), had a residence time of only 0.46 ± 0.06 h, indicating that high potency does not necessarily correlate with slow dissociation.

A comparison of both enantiomers of the methylpyrrolidine linker (**4** and **7**) revealed that the *S*-configuration provided greater durability (**Fig. 2b**). Maintaining the *S*-methylpyrrolidine linker, we revisited the capping group. This led to the discovery that inhibitors containing polar, branched-alkyl capping substituents, exemplified by morpholine **8** and oxetane **9** (**Fig. 2a**), demonstrated further increases in residence time. With a residence time of 167 ± 21 h (1 week) (**Fig. 2b**), **9** is, to our knowledge, among the most durable reversible inhibitors yet identified[2,3]. Trypsinization of the complex formed between BTK and **9** led to quantitative recovery of unaltered **9**, confirming complete reversibility (**Supplementary Fig. 8**).

Examination of 21 cyanoacrylamide-containing pyrazolopyrimidines (**4** and **7**–**26**; **Supplementary Table 1**) revealed a graded continuum of BTK occupancy 24 h after addition of the competitive tracer (**Fig. 2d**); discrete differences in BTK occupancy were also evident at earlier time points (**Supplementary Table 1**). Thus, residence time was tuned across a wide dynamic range via subtle structural perturbations in the linker and branched-alkyl capping group. Little correlation was observed between durability and IC_{50} values in the BTK enzyme assay, consistent with the general inability of IC_{50} measurements to capture the true binding affinity of slow off-rate compounds (**Fig. 2c**). It is unlikely that inhibitors like **9** would have been prioritized with a strategy that focused solely on optimizing IC_{50} values rather than residence time.

Several approaches were used to corroborate the prolonged residence time observed for **9**. First, the rate at which BTK enzymatic activity recovered after incubation with compound followed by dialysis was measured. Compound **9** demonstrated durable BTK inhibition, with only 25% recovery of activity after 3 d of dialysis at room temperature (**Supplementary Fig. 9**). Compound **4** was also durable, but to a lesser extent, reflecting the same ranking as in the off-rate assay. In separate experiments, **9** demonstrated time-dependent inhibition of BTK enzymatic activity (**Supplementary Figs. 10** and **11**), as expected for an inhibitor with an extremely slow off rate. We determined maximal inactivation (k_{inact})/K_i values for compounds **4**–**9** and found that, similar to the IC_{50} values, k_{inact}/K_i did not correlate with residence time (**Supplementary Fig. 11**).

Durability of reversible covalent BTK inhibitors in cells

Cellular potency and durability were assessed on the basis of the ability of inhibitors to block binding of the probe PP-BODIPY to BTK. Preincubation of Ramos B cells with **4**, **7**, **9** and PP-ir blocked BTK labeling in a dose-dependent manner (**Fig. 3a** and **Supplementary Figs. 12** and **13**). To test for durable BTK occupancy, we incubated cells with **9**, washed them extensively to remove unbound inhibitor and incubated them with PP-BODIPY 4 h after the removal of **9**. Compound **9** was equally effective at inhibiting PP-BODIPY labeling with and without washout (**Fig. 3a**), indicating durable interaction. The ability of **4**–**9** to block PP-BODIPY in Ramos cells was next compared 4 and 18 h after washout, and a correlation was observed between biochemical residence time and durable occupancy in cells (**Fig. 3b** and **Supplementary Fig. 14**). We developed a higher-throughput method for determining cellular BTK occupancy using an irreversible, biotin-labeled probe (**27**, PP-biotin; **Supplementary Fig. 15a**) and AlphaScreen technology[36] (**Supplementary Fig. 15b**). Inhibitors **4**, **7**, **8**, **9** and PP-ir blocked PP-biotin binding to BTK with IC_{50} values from 5 ± 1 nM to 27 ± 11 nM (**Supplementary Fig. 15c**). A washout experiment using AlphaScreen detection indicated that reversible covalent BTK inhibitors had varying degrees of durability in Ramos cells, similar to findings for biochemical residence time, with **9** being the most durable (59% ± 17% occupancy 18 h after washout; **Fig. 3c**). Cotreatment with the protein-synthesis inhibitor cycloheximide indicated that much of the apparent recovery of unoccupied BTK during the 18-h washout period was due to BTK turnover and resynthesis in Ramos B cells rather than compound dissociation (**Supplementary Fig. 16**).

BTK occupancy led to diminished signaling downstream of the B cell receptor, as revealed by a flow cytometry–based assay of CD69 expression. In human whole blood, BTK inhibitors including **9** blocked

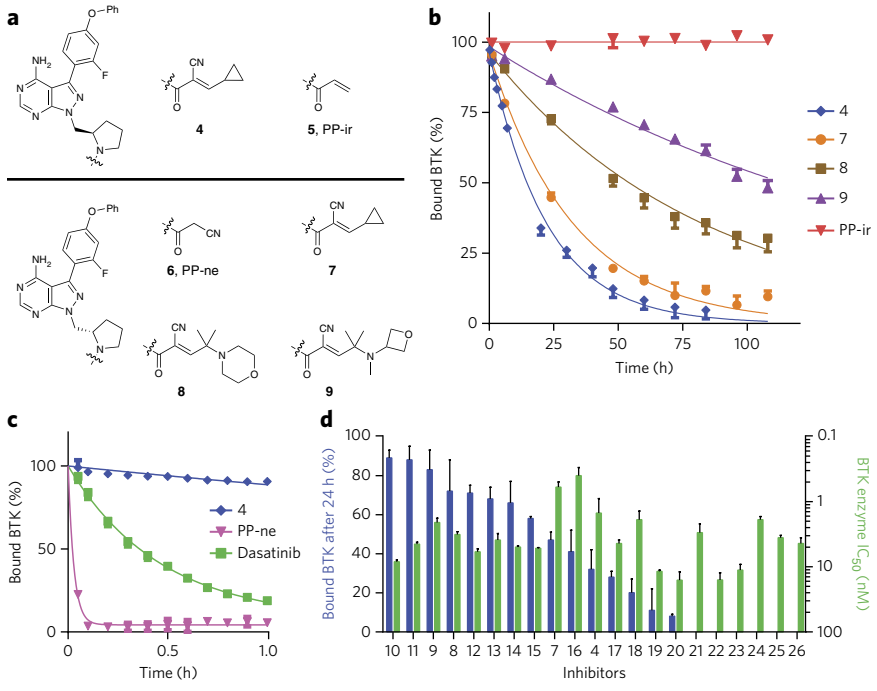

Figure 2 | Prolonged and tunable residence time of reversible covalent BTK inhibitors. (**a**) BTK inhibitors with methylpyrrolidine linkers characterized during residence time–based optimization. Compounds contained *R* (**4** and **5**) and *S* (**6**–**9**) linker configurations. Inhibitors **4**, **7**, **8** and **9** contained a cyanoacrylamide electrophile; PP-ir contained an acrylamide electrophile; and PP-ne had no electrophile. (**b**) Dissociation curves of BTK inhibitors. Shown is the percentage of BTK bound by inhibitor versus time for a 108-h dissociation experiment. Residence times τ were as follows: **4**, 22 ± 3 h; **7**, 34 ± 5 h; **8**, 83 ± 14 h; **9**, 167 ± 21 h; PP-ir, >200 h (mean ± s.d., n = 4). (**c**) Results of a 1-h inhibitor dissociation study. Residence times τ were as follows: PP-ne, <0.1 h; dasatinib, 0.46 ± 0.6 h (mean ± s.d., n = 4). (**d**) Prolonged residence times were tunable and not predicted by enzyme IC_{50} potency. A series of 21 cyanoacrylamide-containing pyrazolopyrimidines with pyrrolidine linkers were characterized both for occupancy after 24 h in the biochemical off-rate assay (blue) and for potency in a BTK enzymatic-activity assay (green). The occupancy at 24 h in the off-rate assay is plotted side by side with the IC_{50} for each compound (mean ± s.d., n = 4). Compounds are arranged in order of descending durability from left to right along the *x*-axis; also see **Supplementary Table 1**. Data are representative of two experiments in **b**–**d**.

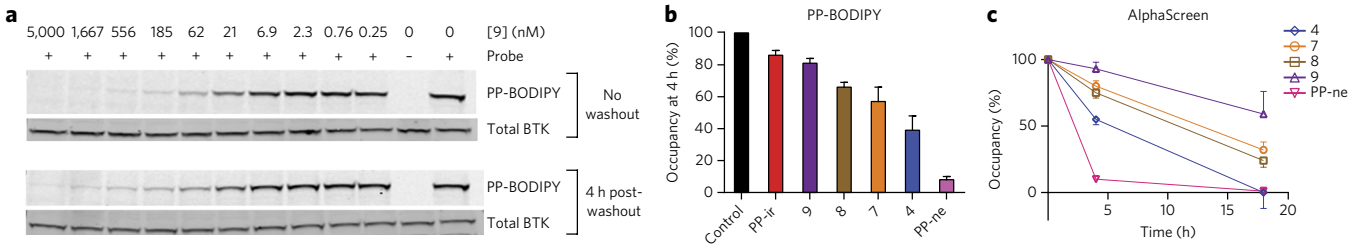

Figure 3 | Long-term cellular durability of reversible covalent BTK inhibitors. (**a**) Sustained BTK occupancy of **9** in cells 4 h after inhibitor washout. Ramos B cells were incubated with various concentrations of **9** and either treated with 1 μM PP-BODIPY directly (top) or washed three times and returned to culture for 4 h before 1 μM PP-BODIPY was added (bottom). Lysates were evaluated for both binding of PP-BODIPY to BTK (PP-BODIPY) and total BTK by western blot. Full gel images are in **Supplementary Figure 25**. (**b**) Reversible covalent BTK inhibitors showed distinct levels of durability in cells. Ramos B cells were incubated with 1 μM inhibitor, washed three times and returned to culture for 4 h before the addition of 1 μM PP-BODIPY. Lysates were evaluated for both binding of PP-BODIPY and total BTK to calculate the percent occupancy of the inhibitor (**Supplementary Fig. 14**) (mean ± s.d., $n = 4$). (**c**) BTK occupancy of reversible covalent inhibitors 4 h and 18 h after cell washout evaluated using AlphaScreen technology (**Supplementary Fig. 15**) (mean ± s.d., $n = 4$). Data are representative of two experiments in all panels.

CD69 expression after stimulation of the B cell receptor with anti–immunoglobulin M (IgM) (**Supplementary Figs. 17** and **18**). Potent BTK inhibition in cells required Cys481, as a C481S BTK mutant transfected into HEK293 cells was >50-fold less sensitive to **9** than wild-type BTK (**Supplementary Fig. 19**).

BTK inhibitor selectivity and *in vivo* residence time

To evaluate kinase selectivity, we tested **9** at concentrations of 1 μM and 0.1 μM in a 254-kinase panel and determined enzyme IC_{50} values (**Fig. 4** and **Supplementary Fig. 20**). Because BTK Cys481 is conserved in only ten other kinases (BLK, BMX, EGFR, ERB-B2, ERB-B4, ITK, MKK7, JAK3, TEC and TXK), we hypothesized that **9** would inhibit a subset of these kinases without affecting kinases that lack this cysteine. Indeed, 1 μM **9** induced >90% inhibition in only 6 of 254 kinases (**Fig. 4a** and **Supplementary Table 2**); these sensitive kinases (BTK, BLK, BMX, ERB-B4, TEC and TXK) share the conserved cysteine as well as a threonine in the gatekeeper position. Only BTK and BMX were inhibited by >90% at 0.1 μM **9** (**Fig. 4a** and **Supplementary Table 3**). Importantly, other kinases that have Cys481 and are known to have critical tissue-specific homeostatic roles (EGFR, ERB-B2, ITK and JAK3) were unaffected by **9** (IC_{50} > 3 μM; **Fig. 4b**). Compound **9** failed to inhibit signaling downstream of EGFR and the T cell receptor (**Fig. 4c**), indicating selectivity in cells for the B cell receptor pathway.

We asked whether the sustained residence time of **9** in biochemical and cellular experiments translated into a prolonged pharmacodynamic effect in rodents. PP-BODIPY was used to determine the level of BTK target engagement in rat peripheral blood mononuclear cells (PBMCs) at several times after oral dosing with 40 mg kg^{-1} **9**. Levels of **9** in plasma were determined simultaneously to assess whether BTK occupancy was driven by prolonged residence time or high levels of **9** in circulation. The plasma level of **9** peaked at 104 ± 66 ng ml^{-1} 1 h after dosing and fell to 24 ± 17 ng ml^{-1} at 6 h and 3 ± 3 ng ml^{-1} at 14 h (**Fig. 5**). As the IC_{50} of **9** in human whole blood was 146 ± 10 ng ml^{-1} (corresponding to 240 ± 20 nM; **Supplementary Fig. 18**), it seemed unlikely that the low plasma levels observed after 6 h could drive BTK target engagement. Assessment of BTK occupancy revealed that 74% ± 9%, 82% ± 5%, 57% ± 9% and 41% ± 15% of BODIPY probe labeling was blocked at 1 h, 6 h, 14 h and 24 h after dosing, respectively (**Fig. 5**). Thus, despite being cleared from the circulation, **9** showed significant target engagement 24 h after oral dosing, reflecting its slow dissociation from BTK *in vivo*.

Prolonged, tunable residence time of FGFR inhibitors

We sought to show that the strategy of tuning inhibitor residence time by varying cyanoacrylamide capping groups is generalizable beyond BTK. Cys486 of FGFR1, located in the kinase P loop, has previously been targeted with acrylamide-based irreversible

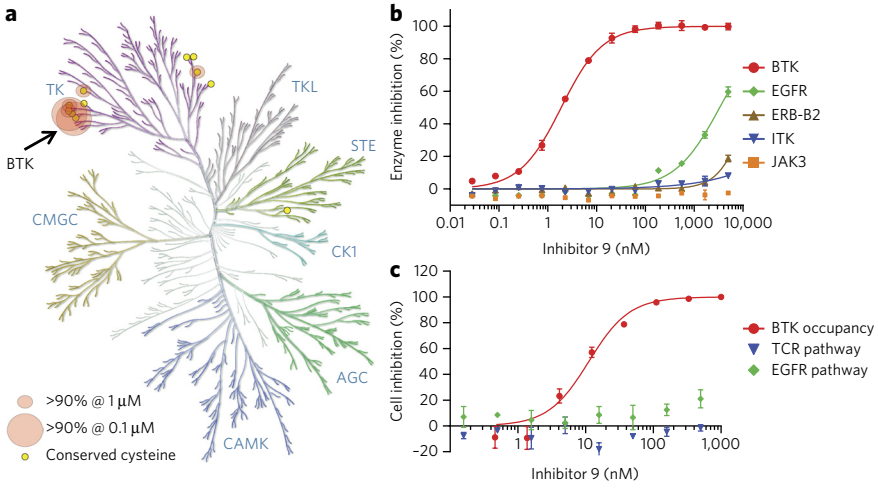

Figure 4 | Kinase selectivity of inhibitor 9. (**a**) Kinase selectivity of **9** evaluated at 1 μM and 0.1 μM in the Nanosyn 254-kinase panel. Small red circles indicate the six kinases that showed >90% inhibition at 1 μM. Large red circles indicate the two kinases (BTK and BMX) that also demonstrated >90% inhibition at 0.1 μM. This figure was reproduced courtesy of Cell Signaling Technology, Inc. (http://www.cellsignal.com). (**b**) Enzymatic IC_{50} curves for **9** used with BTK and other kinases possessing a homologous cysteine that have known tissue-specific homeostatic roles (EGFR, ERB-B2, ITK and JAK3) (mean ± s.d., $n = 4$). IC_{50} values and curves for the other related cysteine-containing kinases are shown in **Supplementary Figure 20**. (**c**) Cellular selectivity of **9**. The activity of **9** in Ramos B cells in a BTK occupancy assay (**Supplementary Fig. 15**) was compared with the activity toward ITK and EGFR in T cell receptor (TCR) and EGFR cellular reporter assays, respectively (mean ± s.d., $n = 4$). In the TCR assay, **9** was studied in a Jurkat T cell line stimulated with anti-CD3 plus anti-CD28 (to activate the T cell–receptor pathway) and NFAT reporter expression was measured. In the EGFR assay, **9** was studied in ME-180 cervical carcinoma cells stimulated with EGF (to activate the EGFR-receptor pathway) and AP-1 reporter expression was measured. Data are representative of two experiments in **b** and **c**.

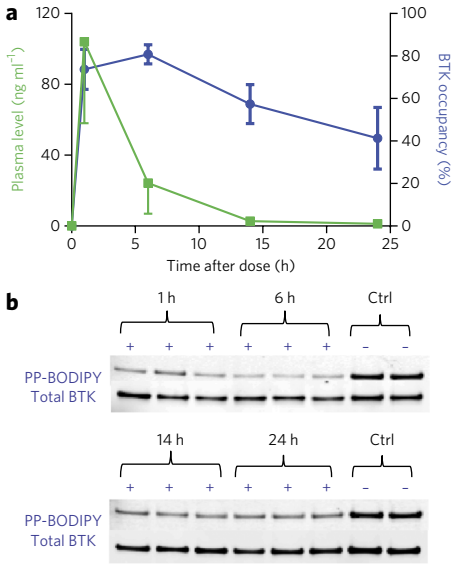

Figure 5 | Extended pharmacodynamic effect of an orally bioavailable BTK inhibitor. (**a**) Pharmacokinetic-pharmacodynamic relationship for **9** in rats dosed orally at 40 mg kg^{-1}. The percent BTK occupancy (in blue) and the concentration of **9** in plasma (in green) at each measured time point after dosing is shown (mean ± s.d., n = 3). The potency of **9** in a human whole-blood assay of CD69 expression was 146 ± 10 ng ml^{-1}. (**b**) The gel-based data used to calculate the BTK occupancy of **9**. Occupancy was determined with in-gel fluorescence using rat PBMCs collected from three separate animals at each time point. The percent BTK occupancy was determined from the percent blocking of BODIPY probe compared to values in vehicle-treated animals (Ctrl), with all samples normalized for the total amount of BTK as evaluated by western blotting. Data are representative of two experiments. Full gel images are in **Supplementary Figure 25**.

inhibitors using a pyrimidopyridine scaffold[37]. This cysteine's location in an active site region distinct from both Cys481 of BTK and Cys436 of RSK2 (**Fig. 6a**) provided an opportunity to demonstrate cyanoacrylamide-based cysteine targeting in a third distinct protein environment. A series of FGFR1 inhibitors were synthesized that contained the same pyridopyrimidinone core and phenyl linker but a variety of electrophile capping groups. Inhibitors were all potent toward FGFR1 in an enzyme-activity assay ($IC_{50} \leq 6$ nM; **Supplementary Table 4**) but varied dramatically in their residence times, as exemplified by **28**, **29** and **30** (**Fig. 6b**,**c**). Compound **28**, a highly durable inhibitor containing a spirocyclic capping group, maintained FGFR1 occupancy throughout the 24-h assay period ($\tau > 150$ h), whereas the equally potent but noncovalent FGFR inhibitor BGJ398 (ref. 38) dissociated much more rapidly ($\tau = 1.9 \pm 0.4$ h; $IC_{50} = 0.9 \pm 0.1$ nM) (**Fig. 6c**). Likewise, although both **28** and BGJ398 potently blocked fibroblast growth factor–stimulated ERK phosphorylation in human umbilical vein endothelial cells, only **28** maintained inhibition after extensive cell washout, indicating a prolonged residence time in cells (**Supplementary Fig. 21**). The FGFR1 inhibitor series, encompassing compounds **28**–**38** (**Supplementary Table 4**), showed a wide continuum of FGFR1-occupancy levels at 24 h in the kinetic-competition assay (**Fig. 6d** and **Supplementary Table 4**), indicating that simple modifications to the capping group and linker discretely modulated FGFR1 residence time, with values spanning several orders of magnitude, analogous to the pattern seen for the cyanoacrylamide pyrazolopyrimidine series for BTK inhibition (**Fig. 2c**). Excellent kinase selectivity for the FGFR family was also obtained (**Supplementary Fig. 22** and **Supplementary Tables 5** and **6**). Many of the capping groups that provided prolonged residence times on FGFR1 were distinct from those that provided prolonged residence times on BTK, indicating that the unique protein environment of each cysteine residue determines which capping groups provide the greatest durability (**Supplementary Figs. 23** and **24**).

DISCUSSION

By exploiting the intrinsic reversibility and facile tunability of inverted cyanoacrylamide-based inhibitors, we demonstrated that BTK inhibitor residence times can be modulated in a discrete, stepwise manner. The strategy focused specifically on maximizing BTK residence time, rather than binding affinity, and the biochemical and cellular assays reported here are applicable to other therapeutic targets for which optimization of residence time is crucial. Fine-tuning of the cyanoacrylamide capping group and linker attached to a kinase-recognition scaffold culminated in the discovery of **9** (**Fig. 2a**), a reversible BTK inhibitor that bound to the intact kinase with a residence time of 7 d but dissociated rapidly and quantitatively upon BTK proteolysis. Cyanoacrylamide **9** was found to have good aqueous solubility (126 μM at pH 7), be orally bioavailable and provide sustained BTK engagement *in vivo*, lasting 18 h after clearance from the circulation. The apparent increase in the compound's dissociation rate in cells relative to the biochemical assay probably reflects the increased temperature (37 °C versus 23 °C) and dynamics of the intracellular environment, including BTK turnover, re-synthesis and interaction with cellular binding partners. Despite these differences, results from the biochemical assay correlated with durability in cells (**Figs. 2b** and **3**).

A breakthrough came with the discovery that certain branched-alkyl capping groups with polar functionality can be attached to the cyanoacrylamide β-carbon to modulate BTK residence time. Such cyanoacrylamides have little precedent in the chemical literature, and before this work it was unclear whether they would even be stable under physiological conditions. When certain capping groups and linkers are combined, noncovalent interactions with the protein (exemplified by the BTK–**3** crystal structure), as well as conformational restriction proximal to the new covalent bond, increase the kinetic barrier to cysteine elimination and thereby stabilize the complex. Such capped cyanoacrylamides could potentially be used to modulate inhibitor residence times for many other cysteine-containing targets, and here we have demonstrated generalizability beyond BTK by showing that Cys486 of FGFR1 could also be targeted with inverted cyanoacrylamide-based inhibitors (**Fig. 6**). No estimate of the total number of drug targets that contain an accessible cysteine (the 'druggable cysteinome') has yet been reported; however, it has been estimated that 39% of kinases (200 of 518) contain an approachable cysteine in the ATP-binding pocket[15], which suggests that the overall percentage of drug targets amenable to cysteine targeting is considerable.

Although cysteine targeting with inverted cyanoacrylamides is likely to be broadly applicable, there are certain limitations to this approach. First, cyanoacrylamides with branched-alkyl capping groups have a high steric demand, potentially limiting their application with relatively unhindered and solvent-exposed cysteines. Second, although structure-based design is useful for identifying initial scaffolds and linkers that orient the cyanoacrylamide near the targeted cysteine, it is not currently possible to predict which linker–capping group combinations will provide the desired residence time. Nevertheless, because the optimization path involves late-stage installation of both the linker and the capping group onto a preassembled scaffold, fine-tuning of inhibitor residence time is highly efficient. Through different combinations of linkers and capping groups, we synthesized 21 closely related compounds covering a wide range of residence times, all of which inhibited BTK enzyme activity at concentrations in the low nanomolar range (**Fig. 2d** and **Supplementary Table 1**).

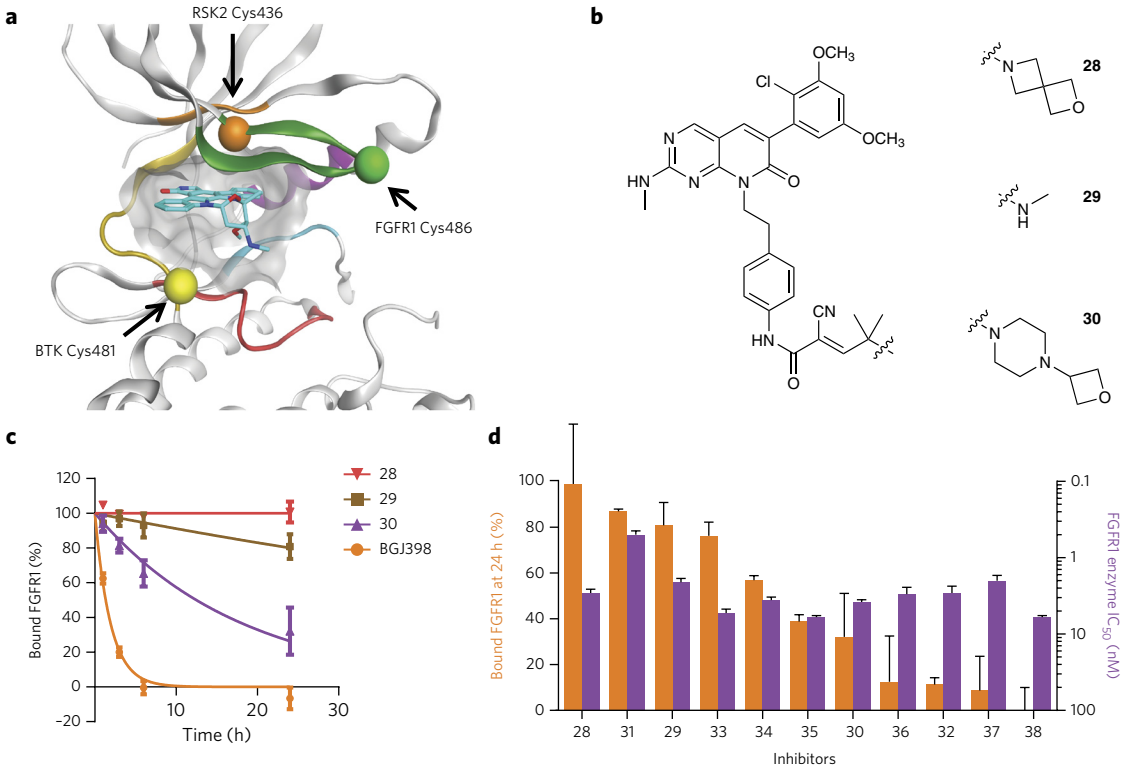

Figure 6 | Inverted cyanoacrylamide FGFR inhibitors with prolonged, tunable residence times. (**a**) Model of the kinase ATP-binding site demonstrating the disparate locations of cysteine residues targeted by cyanoacrylamide-based inhibitors of RSK2, BTK and FGFR1. Structural elements are colored as follows: green, glycine-rich loop; purple, Cα helix; cyan, DFG loop; yellow, hinge region; red, phosphate-binding region. (**b**) Inverted cyanoacrylamides linked to a pyridopyrimidinone scaffold were synthesized with a variety of different capping groups. (**c**) Dissociation curves of FGFR1 inhibitors. Shown is the percentage of FGFR1 bound to the inhibitor versus time for a 24-h dissociation experiment. Residence times τ were as follows: **28**, >150 h; **29**, 110 ± 41 h; **30**, 18 ± 5 h; BGJ398, 1.9 ± 0.4 h (mean ± s.d., n = 4). (**d**) Prolonged and tunable residence time of inverted cyanoacrylamide FGFR inhibitors. FGFR1 inhibitors **28**–**38** containing a variety of electrophile capping groups were characterized (compounds and durability data are shown in **Supplementary Table 4**). Inhibitors demonstrated a continuum of residence times as evaluated by the percent FGFR1 occupancy 24 h after the addition of a fluorescent competitive tracer (orange bars) (mean ± s.d., n = 4). Residence time was not predicted by potency in an FGFR1 enzymatic-inhibition assay (purple bars), as the IC_{50} potency for all compounds clustered in the range between 0.5 ± 0.05 nM and 6.0 ± 0.3 nM. Compounds are arranged in order of descending durability from left to right along the x-axis. Data are representative of two experiments in **c** and **d**.

This study showed that cysteine-targeted, reversible covalent inhibitors can have residence times ranging from minutes to days. For cases in which prolonged residence time on a target is desired, reversible covalent inhibitors may be able to mimic the long-lasting activity of irreversible inhibitors, with dissociation rates *in vivo* that approach the rate of target degradation and re-synthesis. However, molecules with a fast off rate are ideal for certain therapeutic targets because of the mechanism-based toxicity associated with permanent on-target inhibition. Well-characterized examples include the cyclooxygenase inhibitor ibuprofen[39,40], the NMDA-receptor antagonist memantine[41] and the D_2 dopamine–receptor antagonist clozapine[42,43]. For these targets, irreversible inhibition may not be the best approach, but reversible covalent inhibition would still be appropriate. The feasibility of generating a series of ligands with residence times that span a wide temporal range, as demonstrated in this study, suggests that it might be possible to match a ligand's residence time to the biological requirements of a drug target.

BTK has been clinically validated as a target for B cell malignancies through pioneering studies with the acrylamide-based inhibitor ibrutinib[24,25]. In addition to inhibiting BTK and related Tec-family kinases, ibrutinib targets more distantly related kinases, including EGFR, MKK7, ITK and JAK3, that have a cysteine equivalent to BTK Cys481 (refs. 17,28,44). When added to cells at therapeutically relevant concentrations, acrylamide-based probes nearly identical to ibrutinib and a clinical EGFR inhibitor were shown to form irreversible adducts with dozens of other cysteine-containing proteins[28]. Irreversible adducts have historically been a concern in drug discovery because of the relationship between covalent drug binding and the potential for idiosyncratic drug toxicity[10,12,45,46]. Irreversible modification of off-target cysteines may be especially problematic in tissues exposed to high initial drug concentrations after oral administration (often in the micromolar range), such as the gastrointestinal tract and liver. By eliminating the possibility of irreversible binding to off-target proteins, a reversible covalent molecule might provide reduced risk of idiosyncratic drug reactions and therefore be safer than an analogous irreversible inhibitor. Given the intrinsically reversible nature of the cyanoacrylamide-cysteine interaction, the probability that permanent adducts will form with a reversible covalent BTK inhibitor such as **9** is negligible. Moreover, **9** has outstanding kinome-wide selectivity (**Fig. 4**), avoiding all kinases that lack the conserved cysteine and many physiologically important kinases that have this cysteine, including EGFR, ERB-B2, ITK, JAK3 and MKK7.

In addition to their established roles in the treatment of B cell cancers, BTK inhibitors may have beneficial effects in autoimmune diseases. Diseases such as rheumatoid arthritis and lupus erythematosus, which are ameliorated by BTK inhibitors in animal models[17,19,26,27], typically require chronic dosing and a high safety margin, favoring drugs that are highly selective with minimal off-target effects. Reversible covalent BTK inhibitors such as **9** seem well suited for potential use in autoimmune disorders and are

currently being advanced for clinical studies. More broadly, inverted cyanoacrylamides with branched-alkyl capping groups represent a new platform for targeting noncatalytic cysteines. Wide application of this approach has the potential to improve small-molecule residence times across diverse targets and disease areas.

Received 30 October 2014; accepted 13 April 2015; published online 25 May 2015

METHODS

Methods and any associated references are available in the online version of the paper.

References

1. Copeland, R.A., Pompliano, D.L. & Meek, T.D. Drug-target residence time and its implications for lead optimization. *Nat. Rev. Drug Discov.* **5**, 730–739 (2006).
2. Copeland, R.A. The dynamics of drug-target interactions: drug-target residence time and its impact on efficacy and safety. *Expert Opin. Drug Discov.* **5**, 305–310 (2010).
3. Lu, H. & Tonge, P.J. Drug-target residence time: critical information for lead optimization. *Curr. Opin. Chem. Biol.* **14**, 467–474 (2010).
4. Guo, D., Hillger, J.M., IJzerman, A.P. & Heitman, L.H. Drug-target residence time—a case for G protein-coupled receptors. *Med. Res. Rev.* **34**, 856–892 (2014).
5. Swinney, D.C. *et al.* A study of the molecular mechanism of binding kinetics and long residence times of human CCR5 receptor small molecule allosteric ligands. *Br. J. Pharmacol.* **171**, 3364–3375 (2014).
6. Louvel, J. *et al.* Agonists for the adenosine A1 receptor with tunable residence time. A case for nonribose 4-amino-6-aryl-5-cyano-2-thiopyrimidines. *J. Med. Chem.* **57**, 3213–3222 (2014).
7. Vilums, M. *et al.* Structure-kinetic relationships—an overlooked parameter in hit-to-lead optimization: a case of cyclopentylamines as chemokine receptor 2 antagonists. *J. Med. Chem.* **56**, 7706–7714 (2013).
8. Miller, R.M., Paavilainen, V.O., Krishnan, S., Serafimova, I.M. & Taunton, J. Electrophilic fragment-based design of reversible covalent kinase inhibitors. *J. Am. Chem. Soc.* **135**, 5298–5301 (2013).
9. Serafimova, I.M. *et al.* Reversible targeting of noncatalytic cysteines with chemically tuned electrophiles. *Nat. Chem. Biol.* **8**, 471–476 (2012).
10. Barf, T. & Kaptein, A. Irreversible protein kinase inhibitors: balancing the benefits and risks. *J. Med. Chem.* **55**, 6243–6262 (2012).
11. Mah, R., Thomas, J.R. & Shafer, C.M. Drug discovery considerations in the design of covalent inhibitors. *Bioorg. Med. Chem.* **24**, 33–39 (2014).
12. Kalgutkar, A.S. & Dalvie, D.K. Drug discovery for a new generation of covalent drugs. *Expert Opin. Drug Discov.* **7**, 561–581 (2012).
13. Weerapana, E. *et al.* Quantitative reactivity profiling predicts functional cysteines in proteomes. *Nature* **468**, 790–795 (2010).
14. Leproult, E., Barluenga, S., Moras, D., Wurtz, J.M. & Winssinger, N. Cysteine mapping in conformationally distinct kinase nucleotide binding sites: application to the design of selective covalent inhibitors. *J. Med. Chem.* **54**, 1347–1355 (2011).
15. Liu, Q. *et al.* Developing irreversible inhibitors of the protein kinase cysteinome. *Chem. Biol.* **20**, 146–159 (2013).
16. Singh, J., Petter, R.C. & Kluge, A.F. Targeted covalent drugs of the kinase family. *Curr. Opin. Chem. Biol.* **14**, 475–480 (2010).
17. Honigberg, L.A. *et al.* The Bruton tyrosine kinase inhibitor PCI-32765 blocks B-cell activation and is efficacious in models of autoimmune disease and B-cell malignancy. *Proc. Natl. Acad. Sci. USA* **107**, 13075–13080 (2010).
18. Evans, E.K. *et al.* Inhibition of BTK with CC-292 provides early pharmacodynamics assessment of activity in mice and humans. *J. Pharmacol. Exp. Ther.* **346**, 219–228 (2013).
19. Rankin, A.L. *et al.* Selective inhibition of BTK prevents murine lupus and antibody-mediated glomerulonephritis. *J. Immunol.* **191**, 4540–4550 (2013).
20. Benson, M.J. *et al.* Modeling the clinical phenotype of BTK inhibition in the mature murine immune system. *J. Immunol.* **193**, 185–197 (2014).
21. Wu, H. *et al.* Discovery of a potent, covalent BTK inhibitor for B-cell lymphoma. *ACS Chem. Biol.* **9**, 1086–1091 (2014).
22. Akinleye, A., Chen, Y., Mukhi, N., Song, Y. & Liu, D. Ibrutinib and novel BTK inhibitors in clinical development. *J. Hematol. Oncol.* **6**, 59 (2013).
23. Lou, Y., Owens, T.D., Kuglstatter, A., Kondru, R.K. & Goldstein, D.M. Bruton's tyrosine kinase inhibitors: approaches to potent and selective inhibition, preclinical and clinical evaluation for inflammatory diseases and B cell malignancies. *J. Med. Chem.* **55**, 4539–4550 (2012).
24. Byrd, J.C. *et al.* Targeting BTK with ibrutinib in relapsed chronic lymphocytic leukemia. *N. Engl. J. Med.* **369**, 32–42 (2013).
25. Wang, M.L. *et al.* Targeting BTK with ibrutinib in relapsed or refractory mantle-cell lymphoma. *N. Engl. J. Med.* **369**, 507–516 (2013).
26. Di Paolo, J.A. *et al.* Specific Btk inhibition suppresses B cell- and myeloid cell-mediated arthritis. *Nat. Chem. Biol.* **7**, 41–50 (2011).
27. Xu, D. *et al.* RN486, a selective Bruton's tyrosine kinase inhibitor, abrogates immune hypersensitivity responses and arthritis in rodents. *J. Pharmacol. Exp. Ther.* **341**, 90–103 (2012).
28. Lanning, B.R. *et al.* A road map to evaluate the proteome-wide selectivity of covalent kinase inhibitors. *Nat. Chem. Biol.* **10**, 760–767 (2014).
29. Kuglstatter, A. *et al.* Insights into the conformational flexibility of Bruton's tyrosine kinase from multiple ligand complex structures. *Protein Sci.* **20**, 428–436 (2011).
30. Marcotte, D.J. *et al.* Structures of human Bruton's tyrosine kinase in active and inactive conformations suggest a mechanism of activation for TEC family kinases. *Protein Sci.* **19**, 429–439 (2010).
31. Evans, D.A., Ennis, M.D., Le, T., Mandel, N. & Mandel, G. Asymmetric acylation reactions of chiral imide enolates. The first direct approach to the construction of chiral β-dicarbonyl synthons. *J. Am. Chem. Soc.* **106**, 1154–1156 (1984).
32. Lebakken, C.S. *et al.* Development and validation of a broad-coverage, TR-FRET-based kinase binding assay platform. *J. Biomol. Screen.* **14**, 924–935 (2009).
33. Motulsky, H.J. & Mahan, L.C. The kinetics of competitive radioligand binding predicted by the law of mass action. *Mol. Pharmacol.* **25**, 1–9 (1984).
34. Copeland, R.A. *Evaluation of Enzyme Inhibitors in Drug Discovery: A Guide for Medicinal Chemists and Pharmacologists*, 2nd edn. (John Wiley & Sons, 2013).
35. Hantschel, O. *et al.* The Btk tyrosine kinase is a major target of the Bcr-Abl inhibitor dasatinib. *Proc. Natl. Acad. Sci. USA* **104**, 13283–13288 (2007).
36. Eglen, R.M. *et al.* The use of AlphaScreen technology in HTS: current status. *Curr. Chem. Genomics* **1**, 2–10 (2008).
37. Zhou, W. *et al.* A structure-guided approach to creating covalent FGFR inhibitors. *Chem. Biol.* **17**, 285–295 (2010).
38. Guagnano, V. *et al.* FGFR genetic alterations predict for sensitivity to NVP-BGJ398, a selective pan-FGFR inhibitor. *Cancer Discov.* **2**, 1118–1133 (2012).
39. Selinsky, B.S., Gupta, K., Sharkey, C.T. & Loll, P.J. Structural analysis of NSAID binding by prostaglandin H2 synthase: time-dependent and time-independent inhibitors elicit identical enzyme conformations. *Biochemistry* **40**, 5172–5180 (2001).
40. Swinney, D.C. Can binding kinetics translate to a clinically differentiated drug? From theory to practice. *Lett. Drug Des. Discov.* **3**, 569–574 (2006).
41. Lipton, S.A. Paradigm shift in neuroprotection by NMDA receptor blockade: memantine and beyond. *Nat. Rev. Drug Discov.* **5**, 160–170 (2006).
42. Vauquelin, G., Bostoen, S., Vanderheyden, P. & Seeman, P. Clozapine, atypical antipsychotics, and the benefits of fast-off D2 dopamine receptor antagonism. *Naunyn Schmiedebergs Arch. Pharmacol.* **385**, 337–372 (2012).
43. Kapur, S. & Seeman, P. Antipyschotic agents differ in how fast they come off the dopamine D2 receptors. Implications for atypical antipsychotic action. *J. Psychiatry Neurosci.* **25**, 161–166 (2000).
44. Dubovsky, J.A. *et al.* Ibrutinib is an irreversible molecular inhibitor of ITK driving a Th1-selective pressure in T lymphocytes. *Blood* **122**, 2539–2549 (2013).
45. Nakayama, S. *et al.* A zone classification system for risk assessment of idiosyncratic drug toxicity using daily dose and covalent binding. *Drug Metab. Dispos.* **37**, 1970–1977 (2009).
46. Takakusa, H. *et al.* Covalent binding and tissue distribution/retention assessment of drugs associated with idiosyncratic drug toxicity. *Drug Metab. Dispos.* **36**, 1770–1779 (2008).

Acknowledgments

This work was supported by the US National Institutes of Health (NIH) (grants GM071434 to J.T. and F32GM087052 to J.M.M.), the University of California San Francisco (UCSF) Stephen & Nancy Grand Multiple Myeloma Translational Initiative (to J.T.), the Academy of Finland (to V.O.P.) and the Sigrid Juselius Foundation (to V.O.P.). We acknowledge the UCSF Mass Spectrometry Facility (supported by NIH grant P41RR001614).

Author contributions

J.M.M., V.O.P. and J.T. designed experiments involving compounds 1–3; J.M.M. and V.O.P. performed experiments and analyzed data for those compounds. J.M.B., A.B., D.T., V.T.P., S.R., P.A.N., D.E.K., M.E.G., J.O.F., T.D.O., E.V., K.A.B., R.J.H. and D.M.G. designed and managed experiments involving compounds 4–46; J.M.B., A.B., D.T., V.T.P., S.R., D.F., J.S., V.P., T.T., X.L. and D.G.L. performed experiments and analyzed data for those compounds. J.M.B. and J.T. wrote the manuscript with feedback from other authors, and all authors read and approved the manuscript.

Competing financial interests

The authors declare competing financial interests: details accompany the online version of the paper.

Additional information

Supplementary information and chemical compound information is available in the online version of the paper. Reprints and permissions information is available online at http://www.nature.com/reprints/index.html. Correspondence and requests for materials should be addressed to J.M.B. or J.T.

ONLINE METHODS

Chemical synthesis. The synthesis of compounds is described in the **Supplementary Note**.

BTK kinase domain cloning, expression and purification. Human BTK kinase domain (residues 382–659) was inserted into pFastBac-1 by InFusion cloning according to the manufacturer's protocol (Clontech). During PCR amplification, a TEV-cleavable 6×-His tag was introduced on the BTK N terminus. This plasmid was then used to transform DH10α MultiBac cells for preparation of the expression bacmid. Sf21 cells purchased from Invitrogen and used without further authentication or mycoplasma testing were transfected with the MultiBac bacmid using Fugene HD transfection reagent according to the manufacturer's instructions (Roche), and virus was propagated in accordance with published methods. Expression of the BTK kinase domain was subsequently induced in Sf21 cells by infection of 2.0 l of cultured cells with 20 mL virus solution such that cell growth was halted immediately. The cells were collected by centrifugation (800*g* for 15 min), and the pellets were resuspended in 50 mL lysis buffer (50 mM Hepes, pH 7.5, 400 mM NaCl, 1.5 mM DTT) supplemented with 1× protease inhibitor cocktail (Roche). The cells were lysed by five passes through a cell homogenizer. The cellular debris was pelleted by centrifugation (30,000*g* for 30 min). The protein was bound in batch to nickel–nitrilotriacetic acid agarose beads in binding buffer (lysis buffer + 20 mM imidazole) for 4 h at 4 °C. The beads were washed with additional binding buffer (four 5-mL washes), and the protein was eluted with three 0.5-mL portions of elution buffer (lysis buffer + 300 mM imidazole). The His tag was cleaved by the addition of AcTev protease with concomitant dialysis overnight into cleavage buffer (50 mM Tris, pH 8.0, 0.5 mM EDTA, 1 mM DTT). The resulting soluble protein was purified further by gel filtration on an S75 column (gel filtration buffer: 20 mM Tris, pH 8.0, 50 mM NaCl, 3 mM DTT). The protein was then concentrated to 16.8 mg/mL, flash-frozen in liquid nitrogen and stored at −80 °C. The final yield was 4 mg of protein.

Crystallization, data collection and structure solution. BTK kinase domain (KD) (6.0 mg/ml, 0.18 mM) was treated with compound **3** (1 mM) in 10% DMSO, and the mixture was incubated on ice for 30 min and then subjected to ultracentrifugation in a TLA100 rotor for 30 min at 90,000 rpm at 4 °C. To grow crystals of BTK KD–**3**, we mixed 1 µL of protein with 1 µL of precipitant solution composed of 0.1 M MES, pH 6.5, 0.2 M $(NH_4)SO_4$, and 30% (wt/vol) PEG 5000 MME at 4 °C. The crystals grew as stacked plates and were crushed, and individual crystals were cryoprotected in mother liquor supplemented with 15% ethylene glycol and frozen in a stream of liquid nitrogen at 100 K. The crystals belonged to the space group $P2_1$ with unit cell parameters a = 43.5 Å, b = 76.1 Å, c = 88.2 Å, α = 90.0°, β = 96.5° and γ = 90.0° and contained two copies of the complex. All data sets were collected on a stream of liquid nitrogen at 100 K at 1.000-Å wavelength on the 8.2.1 beamline of the Advanced Light Source at the Berkeley National Laboratory. Diffraction data were integrated and scaled with the program XDS[47]. The structure of the BTK KD–**3** complex was solved by molecular replacement using data to 2.2 Å and structure 3GEN as a search model in the program Phaser[48] followed by several rounds of manual rebuilding and restrained refinement with the programs Coot[49] and Phenix[50]. The structure refinement converged to R and R_{free} values of 17.4% and 20.8%, respectively, with 96% favored and 0.2% Ramachandran outliers as validated with the Molprobity server[51]. Data collection and refinement statistics are presented in **Supplementary Figure 3**.

Dissociation of compound 3 from BTK after guanidine-mediated unfolding. BTK (1.5 µM in 20 mM Tris, 50 mM NaCl, pH 8.0) or buffer alone was incubated with 1 µM compound **3** (1% DMSO vol/vol final, 10 µL total volume) for 30 min at room temperature. Guanidinium hydrochloride (6 M, 10 µL) was added to each solution, and the mixtures were incubated for 30 min at 37 °C. Acetonitrile (40 µL) was added to each solution, followed by water with 0.1% formic acid (10 µL). The resulting solutions were analyzed by LC-MS/MS, and **3** was quantified using multiple-reaction monitoring and calibration curves (Waters Acquity UPLC/ESI-TQD instrument with a 2.1 × 50 mm Acquity UPLC BEH C_{18} column). The percent recovery of the BTK-containing sample was determined relative to the control sample lacking BTK.

Competition labeling assay in Ramos cells with PP-BODIPY. Ramos cells purchased from ATCC and used without further authentication or mycoplasma testing were grown in RPMI 1640 media supplemented with 10% FBS and penicillin-streptomycin antibiotics under 5% CO_2. Cells (1 mL, 1 × 10^6 to 1.5 × 10^6) in growth media were treated with drug (0.1% DMSO) for 1 h at 37 °C. PP-BODIPY was added to a final concentration of 1 µM, and the cells were incubated for an additional hour at 37 °C. The cells were collected by centrifugation (650*g* for 3 min) and washed with PBS. The cells were flash-frozen in liquid nitrogen and stored at −80 °C. The cell pellets were resuspended in 50 µL CelLytic M (Sigma, C2978) supplemented with 1× Roche complete protease inhibitors and incubated for 15 min at 4 °C. The cellular debris was removed by centrifugation (20,000*g* for 10 min), and the supernatants were normalized for total protein concentration and subjected to SDS-PAGE analysis. The resulting gel was scanned for fluorescence and either probed by western blotting for total BTK (anti–α-BTK (Cell Signaling, C82B8, or BD Biosciences, 611117), 1:500) and α-tubulin (anti–α-tubulin, Sigma, T6199) or stained with Coomassie Brilliant Blue for total protein.

Cellular-durability studies using the PP-BODIPY occupancy probe. Ramos B cells were seeded at a concentration of 1 × 10^6 cells/well in a 12-well plate. Compounds were added to a final inhibitor concentration of 1 µM, and the plates were incubated at 37 °C for 1 h. Cells were washed three times to remove unbound inhibitor and returned to culture for either 4 or 18 h. After the washout period, cells were incubated with 1 µM PP-BODIPY for 1 h at 37 °C for evaluation of inhibitor occupancy. Cells were pelleted and washed with PBS once, and 40 µL of lysis buffer (CelLytic M, Sigma, C2978) was added to each well. To evaluate the occupancy of BTK with PP-BODIPY and the total amount of BTK present in each sample, we analyzed gels by fluorescent scanning and western blotting as described above. To evaluate the dependence of BTK occupancy on new protein synthesis, we added 100 µL of cycloheximide (50 µg/ml) or culture media alone (10% FBS–RPM1 1600) to 900 µL of cells for 30 min at 37 °C to a final concentration of 5 µg/ml cycloheximide, and then added BTK inhibitors.

Biochemical residence time using fluorescence competition. Using an assay buffer of 50 mM Hepes, pH 7.5, 10 mM $MgCl_2$, 0.01% Triton X-100 and 1 mM EGTA, we added 1 µL of 15 µM compound to 9 µL of 0.5 µM BTK (Invitrogen PV3587) in a 96-well polypropylene plate. After 30 min of incubation, the mixture was diluted in assay buffer. A dilution of 25-fold was used for time-course studies with **4**–**9**, and a fivefold dilution was used for occupancy determinations measured at 1, 6 and 24 h; varying the dilution in this range was demonstrated to have a negligible effect on the determination of BTK occupancy. 10 µL of diluted mixture was transferred to a Greiner 384-well black plate. Europium-coupled Anti-6×His (PerkinElmer, AD0205) and Tracer 178 (Invitrogen, PV5593) were added to final concentrations of 15 nM and 0.75 µM, respectively, in a 20-µL volume. Data were acquired using a PerkinElmer Envision plate reader (Model 2101) containing excitation and emission filters compatible with LANCE time-resolution fluorescence resonance energy transfer. Fluorescence at 665 nM and 615 nM wavelengths was collected at various times. In each experiment, a condition that provided the maximum signal (max) was acquired consisting of the signal from enzyme, Europium-coupled Anti-6×His, and Tracer 178 in the absence of test compound. A background signal (bkg) was also acquired, for which a 1-µM concentration of PP-ir was added to completely block binding of Tracer 178. Data for each test compound were reported as the percentage of bound BTK, which was calculated as 100 × (1 − (cmpd − bkg)/(max − bkg)). To determine the k_{off} value and residence time τ, we used GraphPad Prism software to fit data with a decreasing exponential function of the following form: % occupancy = (100 − Plateau) × exp(−k_{off} × time) + Plateau. The residence time τ was determined as $\tau = 1/k_{off}$. The procedure used for biochemical residence-time studies with FGFR1 (Invitrogen, PV4105) was similar, except that a 60-min enzyme-compound incubation time was used, the dilution after preincubation was 100-fold and a Cy5-labeled pyridopyrimidinone was used as a tracer.

Enzymatic IC_{50} assays. Inhibitor potency in a BTK enzymatic assay was determined using the microfluidic-based LabChip 3000 Drug Discovery System from Caliper Life Sciences, which uses capillary electrophoresis to separate phosphorylated and nonphosphorylated peptides. First 12 concentrations of inhibitor were preincubated with BTK for 15 min. Enzyme, inhibitor, peptide substrate, and cofactors (ATP and Mg^{2+}) were then combined and incubated at 25 °C. The final buffer was 100 mM HEPES, pH 7.5, 0.1% BSA, 0.01% Triton X-100, 1 mM DTT, 10 mM $MgCl_2$, 10 µM sodium orthovanadate, 10 µM β-glycerophosphate, 16 µM ATP and 1% DMSO. At the end of the

doi:10.1038/nchembio.1817

incubation, the reaction was quenched by an EDTA-containing buffer. We evaluated negative controls (containing no inhibitor) and positive controls (acquired in the presence of 20 mM EDTA) simultaneously to calculate the percent inhibition at each compound concentration. We determined the IC_{50} values by fitting the inhibition curves using a four-parameter sigmoidal dose-response model using XLfit 4 software (IBDS). To measure the effect of preincubation time on compound IC_{50}, we modified the above protocol such that the preincubation time for compound and BTK enzyme was 0 min, 10 min, 30 min, 90 min or 180 min. The determination of enzymatic IC_{50} values for BLK, BMX, EGFR, ERB-B2, ERB-B4, ITK, JAK3, MKK7, TEC and TXK was performed as described above, except that the concentration of kinase, the peptide substrate and the ATP concentration were optimized for each kinase. Enzymatic IC_{50} data were acquired by Nanosyn, Inc. (Santa Clara, CA; www.nanosyn.com).

BTK progress-curve analysis. Progress curves of BTK peptide phosphorylation were acquired at six concentrations. The real-time curves were obtained for a total of 5 h using a climate-controlled Caliper LabChip instrument. We used XLfit4 software to fit the curves to the time-dependent inhibition equation $[P] = V_s \times t + ((V_i - V_s)/K_{obs}) \times (1 - \exp(-K_{obs} \times t))$, where V_i is the initial velocity, V_s is the steady-state velocity and K_{obs} reflects the rate of inactivation. For rapid-equilibrium compounds, a linear fit was used: $[P] = V_i \times t$. For time-dependent inhibitors, the obtained K_{obs} values were plotted against the compound concentration using either a hyperbolic or a linear fit. From these plots we determined k_{inact} and K_i. Progress-curve data were acquired by Nanosyn, Inc.

Kinase-selectivity panel. Kinase-selectivity determination using a 254-kinase panel was performed by Nanosyn, Inc.

Dissociation of compound 9 from BTK after trypsinization. A mixture of 2 μM BTK (Invitrogen, PV3587) and either **9** (0.6 μM) or PP-ir (0.6 μM) was incubated at room temperature for 60 min in an assay buffer of 20 mM Hepes, pH 7.5, 10 mM $MgCl_2$, 150 mM NaCl, 5% glycerol, 0.05% Triton X-100 and 1 mM 2-mercaptoethanol. In parallel, **9** (0.6 μM) and PP-ir (0.6 μM) were also incubated with the BTK enzyme storage buffer alone (50 mM Hepes, pH 7.5, 150 mM NaCl, 0.5 mM EDTA, 0.05% Triton X-100, 4 mM 2-mercaptoethanol, 50% glycerol). A trypsin stock solution (Sigma, T1426) was prepared to 1 mg/ml in assay buffer. 60 μL of both the enzyme-compound mixture and the storage buffer–compound mixture were added to 120 μL of 1 mg/ml trypsin. Liquid chromatography–mass spectrometry of the samples was performed by the analytical chemistry group of the Molecular Medicine Research Institute (www.mmrx.org). To calculate inhibitor reversibility, we divided the average mass spectrometry peak area of the compound-BTK-trypsin samples by the peak area for the samples containing compound, storage buffer and trypsin to get the percent reversibility.

BTK cell occupancy using AlphaScreen. To treat Ramos B cells with compounds, we cultured a 100-μL sample containing 1×10^6 cells in a 96-well round-bottom polypropylene plate. 10 μL of a 1:3 dilution series of compound prepared in media containing 1.1% DMSO was added in duplicate, and 10 μL of media with 1.1% DMSO alone was added to control wells. The plates were incubated at 37 °C for 1 h. The PP-biotin probe was prepared at 15 μM concentration from a 5 mM stock using media, and 2.5 μL of 15 μM PP-biotin was added to all wells except DMSO control wells to a final concentration of 330 nM. 2.5 μL of media containing 0.3% DMSO was added to DMSO control wells. The plates were incubated for 1 h at 37 °C. Cells were pelleted and washed with PBS once, and 60 μL of lysis buffer (Cell Lytic M, Sigma, C2978) was added to each well. The plate was incubated for 15–20 min on ice and centrifuged for 5 min at 2,000 rpm at 4 °C. The lysate was transferred to a new polypropylene plate and either stored at −80 °C or used immediately. Following the AlphaScreen manufacturer's protocol (Alpha Technology Protein A Detection Kit, PerkinElmer, 6760617C), we prepared 1× buffer, 200 μg/ml acceptor beads, 30 nM BTK antibody (BTK, BD Biosciences, 611117) and 200 μg/ml streptavidin donor beads. We added 5 μL of acceptor beads and BTK antibody to each well. The plate was sealed and incubated at room temperature for 30 min. Then 10 μL of lysate was added and the plate was incubated at room temperature for 30 min. 5 μL of streptavidin donor beads was added to each well in a dark room. The plate was sealed with a plate sealer and incubated at room temperature on a shaker for 30 min. The plate was read using the PerkinElmer Envision Model 2101 plate reader compatible with AlphaScreen. The percent occupancy was calculated from control samples that were either untreated with test compound (maximum signal) or not treated with PP-biotin (minimum signal). We determined IC_{50} values by fitting dose-response curves to a four-parameter sigmoidal function using GraphPad Prism software.

BTK cell durability using AlphaScreen. To treat Ramos B cells with compounds, we cultured 1 ml containing 1×10^6 cells per well in a 12-well polystyrene plate. 100 μL of test compound was added to cells to a concentration of 1 μM, and 100 μL of media with 1.1% DMSO was added to control wells. The plates were incubated at 37 °C for 1 h. Cells were transferred to microfuge tubes, pelleted, washed three times using media and transferred to a new 12-well plate. The plates were incubated for either 4 h or 18 h. The PP-biotin probe was prepared at 15 μM concentration from a 5 mM stock using media, and the probe was added to wells at a concentration of 330 nM. The plate was incubated for 1 h at 37 °C. Cells were pelleted and washed with PBS once, and 60 μL of lysis buffer (Cell Lytic M, Sigma, C2978) was added to each well. Lysates were evaluated for BTK occupancy using AlphaScreen as described above.

Human whole-blood CD69-expression assay. Human whole blood in sodium heparin, collected at Stanford Blood Center through the center's Research Donor Program, was incubated for 1 h at 37 °C, 5% CO_2 in a humidified incubator with a dilution series of compound or 0.5% DMSO alone as a control. Samples were then stimulated with 50 μg/ml goat $F(ab')^2$ anti-human IgM (SouthernBiotech, 2022-14) for 16–18 h in a 37 °C/5% CO_2 humidified incubator. The blood was stained for CD69 antigen expression on human B cells with BD Biosciences antibodies CD20-FITC (555622), CD69-allophycocyanin (5555633), and corresponding isotype controls according to the manufacturer's recommendations. Red blood cells were lysed with 1× BD Biosciences lysis buffer (555899) according to the manufacturer's recommendations. Cells were washed and resuspended in 1% BSA in PBS and analyzed via flow cytometry on a Cytex DxP11 instrument using FlowJo v7.6.4. The percentage of $CD69^+$ cells was plotted as a function of inhibitor concentration and fit to a sigmoidal dose-response curve using GraphPad Prism software to evaluate inhibitor potency.

T cell receptor and EGFR pathway analysis. The T cell receptor–NFAT reporter assay and the EGFR receptor–AP-1 reporter assay were performed by Thermo Fisher Scientific as part of their SelectScreen Pathway Profiling Service.

BTK and BTK(C481S) cell assay. A transient-transfection assay comparing the activity of wild-type BTK to that of BTK(C481S) was performed by Cell Assay Innovations (Beverly, MA) using ClariCELL technology (http://www.cellassayinnov.com). HEK293 cells were transfected with a vector expressing a sequence verified for full-length human wild-type BTK or BTK(C481S) and then dispensed into multiwell plates. Test compounds were added, and cells were incubated for 2 h. The cells were lysed, and ELISA was carried out by capturing the BTK or BTK(C481S) and detecting autophosphorylation levels using a generic antibody to phosphotyrosine. BTK- and BTK(C481S)-dependent kinase activity in these assays was validated with a kinase-deficient BTK(K430R) control.

***In vivo* analysis.** Sprague Dawley outbred female rats (Harlan Laboratories) were used in these studies. All animal procedures were performed in accordance with the Guide for the Care and Use of Laboratory Animals and had prior approval from Principia Biopharma's Institutional Animal Care and Use Committee adhering to Protocol PRN-01-2011. Study animals were dosed orally at 40 mg/kg with **9** formulated as a suspension in 0.5% methylcellulose. Treatment and vehicle groups consisted of three and four animals per group, respectively. BTK occupancy was measured in individual animals in each group, and the data presented are the average from two independent studies. Blood (4–5 ml) was drawn via cardiac puncture for pharmacokinetic-pharmacodynamic analysis. Blood plasma from each animal was analyzed for the level of test compound by LC-MS/MS. Samples were injected on a Shimadzu LC20AD HPLC system connected to a Sciex API4000 QTrap mass spectrometer. A Phenomenex Gemini column (2.1 × 50 mm) was used at 40 °C with a flow rate of 400 μL/min. Mobile phase A was 0.1% formic acid in water, and mobile phase B was 0.1% formic acid in acetonitrile. A linear gradient of 5%–98% B over 2.5 min was used. The mass spectrometer was operated

in positive-ion electrospray mode with multiple-reaction monitoring for maximum sensitivity. Sciex Analyst software (version 1.6) was used for LC-MS/MS instrument control and acquisition. Compound concentration was determined using a standard curve of internal standard versus compound peak area ratio. Rat PBMCs were isolated with GE Ficoll-Paque Plus (17-1440-03) according to the manufacturer's recommendations. Freshly isolated PBMCs (10×10^6 to 20×10^6 cells) were incubated with 1 μM PP-BODIPY for 1 h. Protein lysates were separated on a 4–12% Bis-Tris SDS-PAGE gel. We detected the BTK-associated fluorescence signal by scanning the gel on a Typhoon image scanner (GE Healthcare). Total BTK was subsequently detected via western blotting with a monoclonal antibody to BTK (clone D3H5, Cell Signaling, 8547) and secondary Alexa Fluor 647–conjugated anti-rabbit IgG (H+L) (Invitrogen, A31573). The signal was quantified using ImageQuantTLv7.0 software.

AlphaScreen ERK phosphorylation. Human umbilical vein endothelial cells (HUVECs) were used to determine compound potency via measurement of fibroblast growth factor (FGF)-induced ERK1/2 phosphorylation. Approximately 30,000 cells were seeded per well in a 96-well cell culture plate at 37 °C overnight. Cells were incubated in the recommended HUVEC media with 10% FBS. After 24 h of incubation, cells were grown in serum-free media for 1 h before treatment with compound. Dilutions of compound were added to cells, starting at a concentration of 1 μM and decreasing in tripling dilutions to a final concentration of 0.05 nM, and the cells were then incubated for 1 h at 37 °C. After a 1-h incubation period, cells were stimulated with 50 ng/ml of FGF2 for 10 min. The reaction was stopped by the addition of 100 μl of ice-cold PBS, and cells were washed three times. After being washed, cells were lysed with 50 μL of 1× lysis buffer (pERK SureFire Kit, PerkinElmer). Lysates were incubated in a pERK SureFire reaction mixture for a total of 4 h as recommended by the manufacturer's protocol. At the end of the incubation period, we measured pERK activity using an Envision multilabel reader (PerkinElmer). The raw signal for pERK activity was used to calculate an IC_{50} value as a function of the log compound concentration for each compound using Prism software from GraphPad.

pERK washout assay. HUVECs were prepared at a concentration of 0.5×10^6 cells/well in a six-well plate and seeded overnight. Cells were starved in RPMI medium for 1 h before the addition of compound (at a concentration tenfold greater than the compound IC_{50}) or DMSO for 1 h at 37 °C. Cells were then washed three times to remove unbound inhibitor and returned to culture for 4 h. Following the washout period, cells were stimulated with 50 ng/ml basic FGF (R&D Systems, 233-FB) for 10 min at 37 °C. Cells were pelleted and washed with cold PBS once, and 40 μl of lysis buffer (Cell Lytic M, Sigma, C2978) was added to each tube. The samples were incubated for 15–20 min on ice and centrifuged for 5 min at 2,000 rpm at 4 °C. The lysate was transferred to a new Eppendorf tube and either stored at −80 °C or used immediately. Lysates were added to gel loading buffer and separated using gel electrophoresis. Gels were transferred onto a nitrocellulose membrane and probed for pERK (1:1,000 dilution; Cell Signaling, 4370) and total ERK (1:2,000 dilution; Cell Signaling, 9102).

K_d determination using β-mercaptoethanol. Solutions were prepared containing 0, 0.5, 1.5, 5, 15, 50, 150 and 500 mM β-mercaptoethanol (BME) in a 1:1 mixture of ethanol and PBS (pH 7.4). Aliquots of a 10 mM DMSO stock solution of test compound (4 μL) were separately added to 196-μL aliquots of the above-described ethanol-PBS solutions containing 0 to 500 mM BME. After these solutions had been allowed to stand at room temperature for 1 h, they were analyzed using an Agilent 1200 LC-MS system equipped with a 50 × 2 mm Phenomenex Luna 5-μm C18 100-Å column. Samples were eluted using a gradient of acetonitrile and water, with both solvents containing 0.1% formic acid. Peaks corresponding to parent and BME adduct were identified by their masses, and the percentage of parent in each sample was determined by measurement of the area under the curve for those peaks in the 254-nm UV trace. The percentage of parent was plotted versus the log of the BME concentration using GraphPad Prism to determine a K_d for the reaction. For **9**, parent and BME adduct were not well separated on the LC-MS system, and the percentage of parent was determined on the basis of the area under the curve of the appropriate extracted mass peaks from the positive ion trace.

Rate of BME reversibility. A 10-μL aliquot of a 10 mM DMSO solution of the test compound was added to a 90-μL aliquot of a 15 mM solution of BME in 1:1 PBS-ethanol. After the mixture had been allowed to equilibrate for about 1 h at room temperature, it was analyzed using an Agilent 1200 LC-MS system equipped with a 50 × 2 mm Phenomenex Luna 5 μm C18 100-Å column. The sample was eluted using a gradient of acetonitrile and water, with both solvents containing 0.1% formic acid. Peaks corresponding to parent and BME adduct were identified by their masses, and the percentage of adduct in the sample was determined by measurement of the area under the curve for those peaks in the 254-nm UV trace. This value was used as the $T = 0$ percent adduct. We then diluted the sample tenfold by adding a 50-μL aliquot to a 450-μL aliquot of 1:1 PBS-ethanol. The diluted sample was then immediately injected on the LC-MS system using the same conditions used for the $T = 0$ data point. LC-MS injections were repeated as often as the LC-MS method would allow (approximately every 6 min) for about 30 min. The percentage of adduct for each time point was determined as described above and then plotted and analyzed using GraphPad Prism. For **9**, parent and BME adduct were not well separated by LC-MS, and the percentage of adduct was determined on the basis of the areas under the curve of the appropriate extracted mass peaks from the positive ion trace.

Structure coordinates. The coordinates of the BTK–**3** crystal structure have been deposited in the Protein Data Bank with accession code 4YHF.

47. Kabsch, W. XDS. *Acta Crystallogr. D Biol. Crystallogr.* **66**, 125–132 (2010).
48. McCoy, A.J. *et al.* Phaser crystallographic software. *J. Appl. Crystallogr.* **40**, 658–674 (2007).
49. Emsley, P., Lohkamp, B., Scott, W.G. & Cowtan, K. Features and development of Coot. *Acta Crystallogr. D Biol. Crystallogr.* **66**, 486–501 (2010).
50. Adams, P.D. *et al.* PHENIX: a comprehensive Python-based system for macromolecular structure solution. *Acta Crystallogr. D Biol. Crystallogr.* **66**, 213–221 (2010).
51. Chen, V.B. *et al.* MolProbity: all-atom structure validation for macromolecular crystallography. *Acta Crystallogr. D Biol. Crystallogr.* **66**, 12–21 (2010).

doi:10.1038/nchembio.1817